Tunable-focus liquid microlens array using dielectrophoretic effect

Hongwen Ren and Shin-Tson Wu

College of Optics and Photonics, University of Central Florida, Orlando, Florida 32816
swu@mail.ucf.edu

Abstract: A tunable-focus liquid microlens array based on dielectrophoretic effect was demonstrated. In a lens cell, two immiscible dielectric liquids but with different dielectric constants are sandwiched between electrodes. One electrode has a holed pattern while the other electrode is continuous. The applied voltage generates an inhomogeneous electric field near the hole regions. Owing to such an electric field, the generated dielectric force would separate the low dielectric liquid into many pieces and each piece is pushed to its neighboring hole. After balance, the droplet array is formed in the contracting state surrounded by the high dielectric constant liquid. Each droplet exhibits a lens character. When the voltage is removed, the droplets relax slightly but still keep a certain contact angle. Reactivating the cell will again enforce the droplets to reshape from relaxing to contracting states and, therefore, changing the focal length. Such a lens cell can be fabricated easily and its response time is reasonably fast. Its potential applications in image processing and zoom lens are emphasized.

OCIS codes: (010.1080) adaptive optics; (220.3630) lens; (230.2090) electro-optical devices

References and links

1. T. Nose and S. Sato, "Liquid-crystal microlens with a non-uniform electric field," Liq. Cryst. **5**, 1425-1433 (1989).
2. N. A. Riza and M. C. Dejule, "Three-terminal adaptive nematic liquid crystal lens device," Opt. Lett. **19**, 1013-1015 (1994).
3. H. Ren, Y. H. Fan, and S. T. Wu, "Tunable Fresnel lens using nanoscale polymer-dispersed liquid crystals," Appl. Phys. Lett. **83**, 1515-1517 (2003).
4. H. Ren, Y. H. Fan, S. Gauza, and S. T. Wu, "Tunable-focus flat liquid crystal spherical lens," Appl. Phys. Lett. **84**, 4789-4791 (2004).
5. G. Li, P. Valley, M. S. Giridhar, D. L. Mathine, G. Meredith, J. N. Haddock, B. Kippelen, and N. Peyghambarian, "Large-aperture switchable thin diffractive lens with interleaved electrode patterns," Appl. Phys. Lett. **89**, 141120 (2006).
6. N. Chronis, G. L. Liu, K. H. Jeong, and L. P. Lee, "Tunable liquid-filled microlens array integrated with microfluidic network," Opt. Express **11**, 2370-2378 (2003).
7. K. S. Hong, J. Wang, A. Sharonov, D. Chandra, J. Aizenberg, and S. Yang, "Tunable microfluidic optical devices with an integrated microlens array," J. Micromech. Microeng. **16**, 1660-1666 (2006).
8. J. Chen, W. Wang, J. Fang, and K. Varahramtan, "Variable-focusing microlens with microfluidic chip," J. Micromech. Microeng. **14**, 675-680 (2004).
9. H. Ren and S. T. Wu, "Variable-focus liquid lens," Opt. Express **15**, 5931-5936 (2007).
10. L. Dong, A. K. Agarwal, D. J. Beebe, and H. Jiang, "Adaptive liquid microlenses activated by stimuli-responsive hydrogels," Nature **442**, 551-554 (2006).
11. T. Krupenkin, S. Yang, and P. Mach, "Tunable liquid microlens," Appl. Phys. Lett**. 82**, 316-318 (2003).
12. S. Kuiper and B. H. W. Hendriks, "Variable-focus liquid lens for miniature cameras," Appl. Phys. Lett. **85**, 1128-1130 (2004).
13. M. Vallet, B. Berge, and L. Vovelle, "Electrowetting of water and aqueous solutions on poly(ethylene terephthalate) insulating films," Polymer **37**, 2465-2470 (1996).
14. C. C. Cheng and J. A. Yeh, "Dielectrically actuated liquid lens," Opt. Express **15**, 7140-7145 (2007).
15. S. Gauza, C. H. Wen, S. T. Wu, N. Janarthanan, and C. S. Hsu, "Super high birefringence isothiocyanato biphenyl-bistolane liquid crystals," Jpn. J. Appl. Phys. **43**, 7634-7638 (2004).
16. H. Ren, Y. H. Lin, and S. T. Wu, "Adaptive lens using liquid crystal concentration redistribution," Appl. Phys. Lett. **88**, 191116 (2006).
17. C. C. Cheng, C. A. Chang, and J. A. Yeh, "Variable focus dielectric liquid lens," Opt. Express **14**, 4101-4106 (2006).

#91258 - $15.00 USD Received 3 Jan 2008; revised 7 Feb 2008; accepted 11 Feb 2008; published 12 Feb 2008

18. Http://web.mit.edu/6.013_book/www/chapter11/11.9.html
19. R. A. Hayes and B. J. Feenstra, "Video-speed electronic paper based on electrowetting," Nature **425**, 383-385 (2003).
20. S. Vafaei and M. Z. Podowski, "Theoretical analysis on the effect of liquid droplet geometry on contact angle," Nuclear Engineering and Design **235**, 1293-1301 (2005).

1 . Introduction

Tunable focus adaptive lenses have potential applications for image processing, beam steering, ophthalmology, and cell phone cameras. Although various lenses have been demonstrated, basically they can be grouped into two categories: liquid crystal (LC) lenses [1-5] and liquid lenses [6-14]. In an LC lens, the focal length (f) is dependent on the LC birefringence (Δn), LC layer thickness (d), and radius of lens aperture (r) as $f=r^2/2d\Delta n$. For a given aperture size, increasing the Δn or cell gap helps to shorten the focal length. However, increasing cell gap would lead to an unfavorable slow response time. Thus, using a high birefringence LC [15] is a preferred approach. Realistically speaking, LC is more suitable for making microlens or microlens array than large-aperture lenses.

In comparison to LC lenses, the adaptive liquid lens is based on the change of lens shape. Its optical path length change can be as large as few millimeters, which is about one order of magnitude larger than that of an LC lens. Thus, the liquid lens can present a larger aperture size and its focusing power is stronger. According to the operation mechanism, liquid lenses can be classified into four types: fluidic pressure [6-9], thermal effect [10], electro-wetting [11-13], and dielectrophoresis [14, 16-17]. Among them, electro-wetting and dielectrophoresis (also called dielectric lens) have several common features, e.g., similar lens structure, electrical driving, large focus power change, and fast response time, except that the employed liquids are different. In an electro-wetting lens, the two liquids employed in the lens chamber are immiscible: one is conductive and the other non-conductive. The non-conductive liquid makes a contact angle on the chamber surface. Because the contact angle is electrostatically controllable, the focal length of the lens can be tuned accordingly. As for a dielectric lens, it uses two immiscible dielectric liquids with different dielectric constants. When the two liquids experience an inhomogeneous electric field, the generated dielectric force causes the low dielectric constant liquid to shrink toward the region where the electric field is weaker. Because of the contact interface deformation between these two liquids, the focal length of the lens is tunable. Based on the described operation mechanisms, it is difficult to extend the electro-wetting and dielectrophoretic effects into microlens array. The major challenge is to find a non-mechanical method to form uniform liquid droplet array on the substrate surface.

In this paper, we overcome the technical barrier and demonstrate a tunable-focus liquid microlens array based on the dielectrophoretic effect. Using a hole-patterned electrode, we can easily get a liquid microlens array. The generated dielectric force not only forms but also activates the microlens array. Depending on the patterned electrode structure, a microlens array with variable aperture and density can be designed easily. This kind of lens has compact structure, simple fabrication process and, therefore, is a strong contender for microlens array.

2. Device structure and operation principles

To form a liquid microlens array, two immiscible dielectric liquids are used: the first one (L-1) has a relatively low dielectric constant and high refractive index, while the second one (L-2) has a higher dielectric constant but lower refractive index. Figure 1 illustrates the device fabrication procedures and operation mechanism of the microlens array. In Fig. 1(a), there are six fabrication steps: (1) coating electrode on the surface of a glass substrate, (2) etching the electrode with a hole-array pattern, (3) coating a dielectric layer on the electrode surface, (4) coating L-1 on the dielectric layer, (5) dropping L-2 on the surface of L-1, and (6) laminating the two liquids using an indium tin oxide (ITO) coated glass substrate.

#91258 - $15.00 USD Received 3 Jan 2008; revised 7 Feb 2008; accepted 11 Feb 2008; published 12 Feb 2008

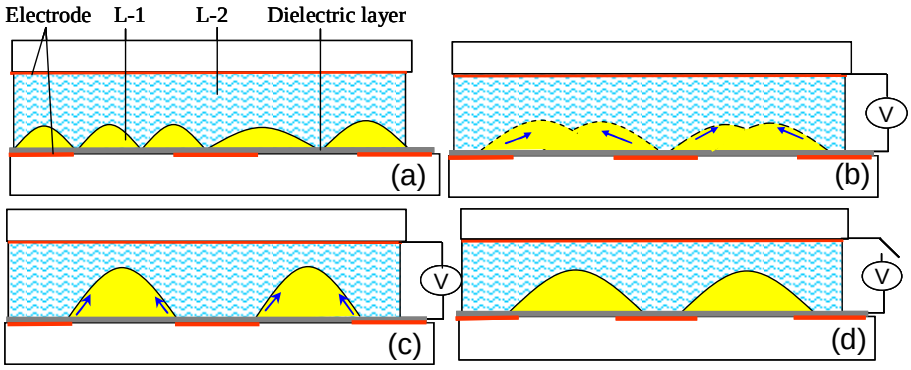

Fig.1. Side view of the droplet array forming processes. (a) two liquid layers, (b) droplet forming process, (c) stable state with a voltage, and (d) in a relaxed state without voltage.

To avoid aggregation of L-1 when the step 4 is finished, steps 5 and 6 should follow immediately. From Fig. 1(a), the formed L-1 layer could be flat, rough, or break into tiny droplets depending on the surface tension of the liquids. As soon as the cell is sealed, a suitable voltage is applied immediately, as shown in Fig. 1(b). Due to the hole electrode, both liquids experience a centro-symmetrical gradient electric field. Near the holes, a dielectric force is generated on the contact surfaces of the two liquids. The dielectric force can be expressed as [18]

$$\vec{F} = \frac{\varepsilon_0}{2}\nabla[(\varepsilon_1 - \varepsilon_2)E \bullet E] - \frac{1}{2}E \bullet E\nabla(\varepsilon_1 - \varepsilon_2) \tag{1}$$

where ε_0, ε_1 and ε_2 are the permittivities of free space, L-1, and L-2, respectively, and E denotes the electric field across the cell gap. Equation (1) contains two parts, but the second term is either negligible or zero because ε_1 and ε_2 are both scalars. Therefore, the electric field gradient plays the key role to the dielectric force. From Eq. (1), the net force is zero when $\varepsilon_1=\varepsilon_2$. Also, the force changes sign depending on whether the droplet's dielectric constant is larger or smaller than that of the surrounding L-2.

When the dielectric force is strong enough, it enforces L-1 and L-2 to redistribute: L-1 is broken up into many droplets and each droplet is attracted by its nearby non-electrode region (as the arrows show). The hole electrode regions function as traps. If two or more L-1 droplets fall off the same trap, they will merge to form one droplet, as shown in Fig. 1(b). As for the L-2, it is squeezed in the high electric field region and surrounds the isolated L-1 droplets. When the redistribution of the two liquid is completed, L-1 will exist as tiny droplets and occupy the weak electric filed regions, as shown in Fig. 1(c). Due to the impact of dielectric force, those droplets are in the contraction state. When the voltage is removed, the droplets will spread out around the electrode holes due to the potential energy balance, as depicted in Fig. 1(d). The adjacent droplets will remain isolated because of the resistance of L-2. The distribution of L-1 is stable on the substrate surface because the following condition is satisfied [19]:

$$\gamma_{w,d} > \gamma_{o,w} + \gamma_{o,d}\,, \tag{2}$$

where γ is the interfacial tension and the subscripts *w*, *o*, and *d* represent the water, oil, and dielectric layer, respectively. When the cell is activated by a voltage again, the droplet surface will return to the shape shown in Fig. 1(c). The droplet profile changing from Fig. 1(d) to Fig. 1(c) makes the focal length of the microlens tunable. Because the size of the isolated liquid droplet is so small, from theoretical analysis the shape of these ultra-small droplets is mainly spherical [20].

In a relaxed state, the droplet makes a contact angle (θ) on the bottom substrate surface, as Fig. 1(d) depicts. Since the shape of the droplet is axially symmetric, the droplet exhibits a lens-like character. In this state, the focal length of the droplet can be expressed as [11]:

#91258 - $15.00 USD Received 3 Jan 2008; revised 7 Feb 2008; accepted 11 Feb 2008; published 12 Feb 2008

$$f^3 = \frac{3V}{\pi(1-\cos\theta)(2-\cos^2\theta-\cos\theta)(n_1-n_2)^3}, \quad (3)$$

where V is the volume of the droplet, and n_1 and n_2 are the refractive indices of L-1 and L-2, respectively. When a voltage is applied to the electrode again, the induced dielectric force will push the droplet and, thus, increase the contact angle. Based on Eq. (3), the focal length of the microlens will change correspondingly.

To demonstrate the liquid microlens array shown in Fig. 1(d), we evaporated a thin aluminum (Al) layer on a glass substrate. The opaque Al layer was then etched with a holed array pattern using photolithographic technique. The aperture of each hole is 140 μm and the gap between the adjacent holes is 100 μm. Then we coated a thin polyimide layer on the Al surface. Here we chose diacrylate monomer AE-93 (n~1.46 and ε~5) as L-1 and de-ionized (DI) water (n=1.33, ε~80) as L-2. The monomer AE-93 has 13 methylene units in the sidechain and its surface free energy is 34.6 mN/M. The L-1 was spun-coated on the polyimide surface and the DI water was dropped on the L-1 surface. An ITO glass substrate was used as top substrate to seal the two liquids. The cell gap was controlled to be ~120 μm. The dielectric polyimide layer used in this cell has two functions: hydrophobic and non-conductive.

After the cell was fabricated, we observed its imaging performance using an optical microscope (Olympus BX51). The cell was placed on the microscope stage which can travel in the vertical direction. Initially, no focusing effect was observed. This means no real L-1 droplets were formed in the hole regions. However, when a voltage (V~60 V_{rms}) was applied for several seconds, each pixel presented a lens character. After the voltage was removed, the lens behavior persisted. Such results imply that the generated dielectric force indeed helps to form the liquid lens.

3. Lens characterizations

Because the lens is micro-sized, it is very convenient to use the optical microscope to evaluate the lens performance. Firstly, we used a microscope to observe the 2D focus spot of the liquid droplets. To easily observe the focus change, we intentionally adjusted the position of the lens cell such that the lens is in a large defocused state, as shown in Fig. 2(a). When an external voltage of ~60 V_{rms} (~300 Hz) was applied to the electrodes, the size of the defocused spot was decreased evidently, as shown in Fig. 2(b). This result indicates that the focal length of the lens is changed. Furthermore, according to Fig. 1(c), one can conclude that the focal length of the lens is shortened. At V= 88 V_{rms}, as shown in Fig. 2(c), the focused spot is the smallest which means the focal length is the shortest. At V=88 V_{rms}, the current intensity was measured to be ~3 μA (DC), corresponding to a power consumption of ~0.26 mW.

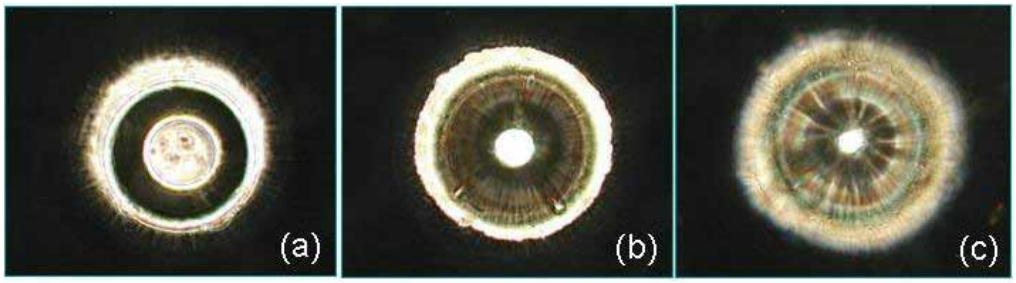

Fig. 2. The voltage dependent focal spot of one pixel lens. (a) 0 V, (b) 60 V, and (c) 88 V.

To observe the image quality of the microlens array, we typed a letter “A” on a piece of transparency as an object. The object was placed under the lens array. By adjusting the

#91258 - $15.00 USD Received 3 Jan 2008; revised 7 Feb 2008; accepted 11 Feb 2008; published 12 Feb 2008

distance between the lens cell and the object, we observed a clear image array in the voltage-off state. Figure 3(a) shows the image (1×3) of the object taken using a digital camera. In contrast to the original object, the image "A" is inverted. One can see that the middle and the right images are very clear but the left one is a little blurred because it is somewhat defocused. As the applied voltage is increased, the images become blurry instantly due to the defocusing effect. Figure 3(b) shows the case for V=60 V_{rms}. The images are very blurry because they are highly defocused. To restore the clarity, we adjusted the cell position while the voltage was still applied to the cell. Figure 3(c) shows the image after refocusing. One can see the images are still very clear except for the reduced size. Because the diameter of each droplet is small (~0.19 mm), their shape is nearly spherical. Therefore, spherical aberration and defocusing are responsible for any incurred image distortion.

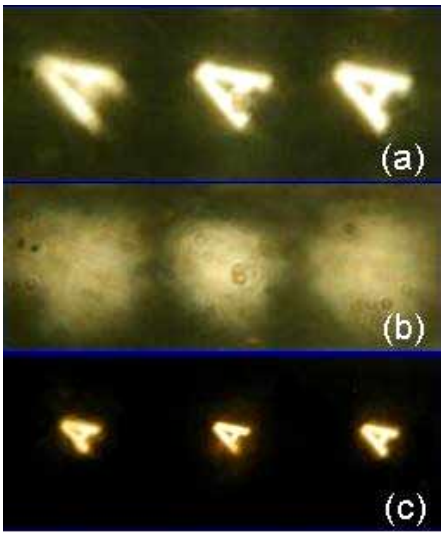

Fig. 3. Imaging properties of the microlens array at (a) V=0, (b) V=60 V, and (c) refocused state.

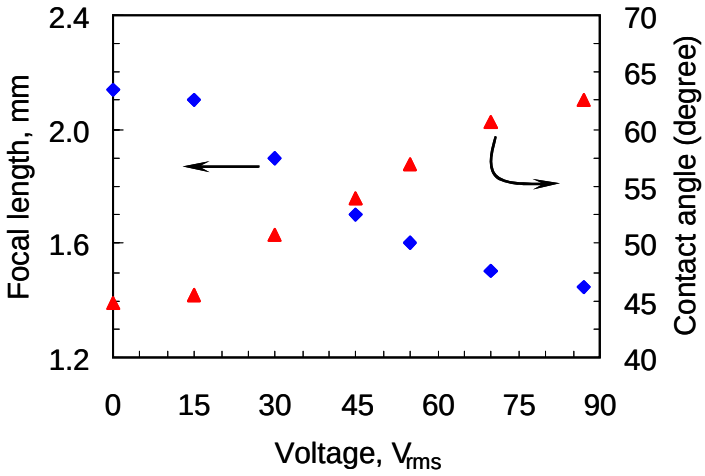

Fig. 4. Voltage dependent focal length and the contact angle.

The focal length of the microlens was measured at different voltages using our optical microscope and results (red triangles) are plotted in Fig. 4. At V=0, the inherent focal length of the lens is f~2.1 mm. From the parameters of the lens cell, i.e., cell gap (~0.12 mm), lens aperture (~0.19 mm), refractive indices of water (n~1.333) and monomer (n~1.46), we calculated (using Code-V program) the radius and apex distance of the droplet to be ~0.28

#91258 - $15.00 USD Received 3 Jan 2008; revised 7 Feb 2008; accepted 11 Feb 2008; published 12 Feb 2008

mm and ~0.08 mm, respectively. Moreover, the volume of the droplet was calculated to be V~ 0.0016π mm^3. As the voltage increases, the focal length is gradually decreased, but the volume remains unchanged. At V=88 V_{rms}, the focal length is decreased to f~1.4 mm. To further widen the dynamic range, we could enlarge the cell gap and the radius of electrode holes. From Eq. (3), the contact angle was also calculated based on the measured focal length. The results are also shown in Fig. 4. At V=0, the contact angle is ~45^o. As the voltage increases to V=88 V_{rms}, the contact angle increases to 62.5^o.

The spherical aberration of the microlens was evaluated using Cove-V according to the parameters of the lens cell and the measured focal length. In the relaxed state (f~2.1 mm), the third order (SA3) and the fifth order (SA5) aberrations were calculated to be 4.95 μm and 0.42 μm, respectively. In the highly contracting state (f~1.45 mm), SA3 and SA5 were found to be 3.59 μm and 0.30 μm, respectively. Because of the relatively large spherical aberration (SA3), this type of lens is not targeted for high resolution applications.

Response time of an adaptive lens is an important parameter for active imaging devices because it determines the data acquisition rate. We measured the response time using a square voltage burst at f=300 Hz and 60 V_{rms}. Similar to Fig. 2(a), at V=0 the lens cell was adjusted in a larger defocused state. The intensity of the incident light was greatly decreased so that only the central spot was observable. To visually observe the tunable focus and the response speed, a movie for tuning a 2×3 microlens array was taken, as shown in Fig. 5. One can see the response speed of all the microlenses is almost the same. The rise time was measured to be ~30 ms and the fall time ~250 ms.

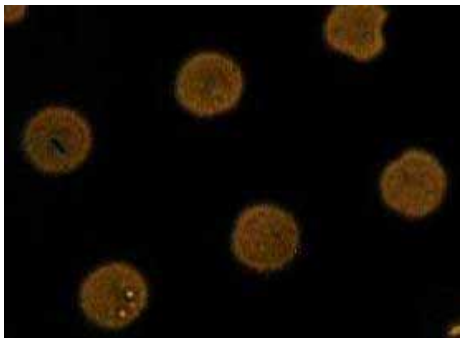

Fig. 5. 2x3 mircolens array driven from a defocused state to a focused state. (755KB)

In this experiment, the DI water was chosen for feasibility demonstration. From Eqs. (1) and (3), DI water is attractive for widening the focal length tunability and decreasing the operating voltage because of its low refractive index and large dielectric constant. However, water freezes at 4^oC. Therefore, for practical applications we need to choose a suitable material to substitute water and, meanwhile, the microlens material should be carefully chosen. Using our proposed method, not only a microlens array can be fabricated easily but also a single miniature lens can be prepared for cell phone cameras. To decrease the operating voltage, we could choose two liquids with a large difference in dielectric constants. And also, the patterned electrode should provide a large gradient electric field.

4. Conclusion

We demonstrated an electrically tunable-focus liquid microlens array using a hole-patterned electrode. The generated dielectric force serves two purposes: helps to form the microlens array, and to change the focal length. In the lens cell, each microlens is a converging lens whose focal length can be tuned electrically. Our lens cell has the advantages of easy fabrication, compact structure, scalable aperture, and electrical control. In comparison to LC based microlens, the liquid microlens has advantages in large focal length tunability, broad spectral bandwidth, and fast response time during focus change.

#91258 - $15.00 USD Received 3 Jan 2008; revised 7 Feb 2008; accepted 11 Feb 2008; published 12 Feb 2008

Acknowledgment

The authors are indebted to Haiqing Xianyu and Meizi Jiao for their experimental assistance.

#91258 - $15.00 USD Received 3 Jan 2008; revised 7 Feb 2008; accepted 11 Feb 2008; published 12 Feb 2008